Volume 20, No 3 | International Journal of Radiation Research, July 2022

Potential implications of the radiation-induced bystander effect for spatially fractionated radiotherapy: A theoretical simulation study

F. Mahmoudi[1], D. Shahbazi-Gahrouei[1*], N. Chegeni[2], M. Saeb[1], V. Sadeghi[3], S. Hemati[4]

[1]Department of Medical Physics, Faculty of Medicine, Isfahan University of Medical Sciences, Isfahan, Iran
[2]Department of Medical Physics, Faculty of Medicine, Ahvaz Jundishapur University of Medical Sciences, Ahvaz, Iran
[3]Department of Biomedical Engineering, Faculty of Advanced Medical Technology, Isfahan University of Medical Sciences, Isfahan, Iran
[4]Department of Radiation Oncology, Faculty of Medicine, Seyyed Al-Shohada Hospital, Isfahan University of Medical Sciences, Isfahan, Iran

► ***Original article***

Corresponding author:
D. Shahbazi-Gahrouei, Ph.D.,
E-mail:
shahbazi24@yahoo.com

Received: July 2021
Final revised: February 2022
Accepted: March 2022

Int. J. Radiat. Res., July 2022; 20(3): 657-664

DOI: 10.52547/ijrr.20.3.20

Keywords: *GRID therapy, spatially fractionated radiotherapy (SFRT), tomotherapy, bystander effect, LATTICE radiotherapy.*

ABSTRACT

Background: It has been found that the bystander effect plays a key role in the survival of cells exposed to highly non-uniform radiation beams. However, the linear-quadratic (LQ) model cannot predict these effects well. The present study aimed to explore the potential impact of the radiation-induced signaling effects on treatment plans for spatially fractionated radiation therapy (SFRT) using a numerical radiobiological model. ***Materials and Methods***: Two tomotherapy-based SFRT plans were created using commercially available software in this work. The tumor response to these plans was modeled by both the conventional LQ model and a bystander model incorporating the indirect effect of radiation. We have investigated how dose-volume histograms (DVHs), dose distribution, equivalent uniform dose (EUD), and mean dose change with radiation-induced signaling effects. ***Results***: When the intercellular signaling effects are included in the predictive survival model, the cell-killing within the low-dose regions of GRID fields increases. This leads to an increase in the EUD and means dose. These effects are more striking for the LATTICE radiotherapy plan, which contains high dose gradients in three dimensions. ***Conclusion***: Incorporating radiation-induced signals in tumor cells response to SFRT significantly deviates from the LQ model predictions. Therefore, it is recommended to use the radiobiological models which take both the signaling and radiation effects into account to predict survival in highly modulated radiation beams, especially in LATTICE radiotherapy.

INTRODUCTION

Spatially fractionated radiation therapy (SFRT) or GRID therapy is a unique delivery technique that has demonstrated promise in achieving enhanced tumor response while still sparing organs at risk when treating deep-seated large tumors. In this modality, a very high non-uniform dose of radiation is given in a single fraction over the tumor volume. In contrast to the conventional methods of radiation therapy, only a fraction of the tumor will receive the primary radiation, and the rest receives a small or no dose [1].

The exact mechanisms behind the benefits of SFRT are not fully understood. While most of the previous studies have been focused on the physical and dosimetric features of the GRID [2-6], induced radiobiological changes such as abscopal and bystander effects were speculated to be of paramount importance well [7-9]. It has been seen that non-directly irradiated cell populations in the shielded area of the SFRT field (bystander cells) experience some off-target effects in response to signals received from directly irradiated cells which challenged the target response idea [1, 9-11].

Although the previous theoretical studies of GRID therapy were generally based on the linear-quadratic (LQ) model for the calculation of local survival and equivalent uniform dose (EUD) [2, 4, 12, 13], the accuracy of this model for highly modulated radiation fields has been questioned. It has been shown that the bystander effects play an important role in the highly modulated radiation field of SFRT. However, local survival is dictated solely by locally delivered doses in the LQ model, and no bystander effects were included. This resulted in a significant deviation of the LQ model predictions from experimental results

[DOI: 10.52547/ijrr.20.3.20]

[14-17]. This study aimed to investigate how radiation-induced signaling effects may have an impact on dose distribution and EUD for a range of tomotherapy-based SFRT. This approach is based on a computational model incorporating radiation and signaling-induced damages. This model has been developed by McMahon *et al.* in 2013 and has shown that it can precisely quantify all of these effects.

The results of this study may have a significant impact on radiotherapy treatment planning for SFRT. They can be used to design experiments required to specify the optimum parameters that lead to the highest therapeutic advantage of SFRT.

MATERIALS AND METHODS

GRID structures

In this study, two types of SFRT plans named virtual TOMOGRID and three-dimensional LATTICE radiotherapy (3-D LRT) templates were created by in -house software, DICOMan (version 5.0.0, the University of Arkansas for Medical Sciences, Little Rock, AR, USA) (18). LRT is a related modern approach of SFRT, in which several high dose regions are delivered in sphere-like vertices inside the target volume with low dose regions in between. At the first step, a virtual cylindrical computed tomography (CT) phantom (32 cm diameter and 40 cm length) was created as an ideal structure of the patient. Then, another cylindrical volume (10 cm diameter and 10 cm length) was placed at the center of the larger cylinder to mimic the gross tumor volume (GTV).

The virtual helical tomotherapy (HT) GRID pattern (HT-GRID) consists of three main structures: GTV, GRID target, and avoidance structure. The GRID target is a structure that is equivalent to the openings of commercially available GRID blocks. The GRID target is used as the target constraint for the plan optimization process to gain high dose regions within the GTV. The avoidance structure is created by extracting the GRID target from the GTV. This structure is equivalent to the shielded area of the conventional GRID block field used as the OAR constraints to reduce the valley dose as much as possible. In addition, we generated an outer shell with three millimeters in thickness around each GRID target to confirm the dose to the targets and control the dose gradient in GTV.

In this study, two different GRID target configurations consisting of a set of equally spaced cylinders (TOMOGRID) and also a lattice of spheres with a hole diameter of 10 mm and center-to-center distance of 30 mm were generated within the GTV in a honey-comb pattern, using DICOMan software (figure 1).

GRID treatment plan

After that, the new structures were created by DICOMan, the phantom's CT images along with the new contours were imported to the helical tomotherapy treatment planning system (HT-TPS). All treatment plans were generated on Accuray Precision; 2.0.1.1 HT-TPS and were designed for delivery on the Radixact-X9 tomotherapy system. A prescription dose of 15 Gy was set to be delivered for each plan in a single fraction using a field width of the 2.5 cm dynamic jaw, a pitch of 0.434, a modulation factor of 3 and 6 MV photon beams [19-21].

To evaluate the dosimetric characteristics of HT-GRID, the valley-to-peak dose ratio (VPDR) was specified. The peak dose was defined as the mean dose to the GRID target. The valley dose was defined as the mean dose to the valley.

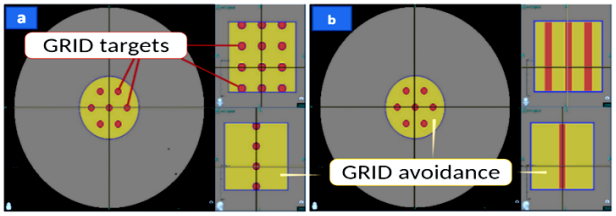

Figure 1. Target arrangement for LRT plan **(a)** and TOMOGRID plan **(b)** consisting of several spheres and cylinders, respectively. Inline and crossline profiles are identified by the arrows. GTV is defined by the blue outline.

Intercellular signaling model

In the bystander model developed by McMahon *et al.* [22, 23], DNA damages are quantified as several hits that accumulate to a sensitive target within the cells and lead to cell death. Hits and damages accumulate both as a function of physical radiation dose as well as bystander signals from adjacent irradiated cells. Although various factors have been speculated to be involved in the radiation-induced intercellular effects, no clear empirical information about the role of different molecules exists, therefore, in this study bystander signal is modeled as a single concentration, ρ. By determining the level of biological damages within each cell, survival can thus be predicted. Full descriptions of the intercellular signaling model are available elsewhere and are briefly summarized below for completeness [23-25].

Cells exposed to ionizing radiation secrete signals for a time (t_{sig}) proportional to the delivered dose (D). This time is calculated using equation (1), where the γ is a cell-specific parameter.

$$t_{sig} = \gamma D \quad (1)$$

These signals are assumed to be unstable, being eliminated from media with decay coefficient λ. So, in uniform irradiations, signal concentration initially builds up towards an equilibrium value. Then the irradiated cells cease signaling and the signal concentration decreases. However, if the cells are exposed to a non-uniform radiation field, the produced signals disperse in media via diffusion

[DOI: 10.52547/ijrr.20.3.20]

while simultaneously decaying. This signal propagation leads to a shift in the signal concentrations and thus biological damages, compared to uniformly irradiated populations.

The degree of the indirect damages caused by the bystander signal is proportional to the time (τ) in which the cell is exposed to the signal above a certain threshold ($\rho_{threshold}$). Thus, the probability of a response to intercellular signaling effects (P_B) is given by equation (2):

$$P_B=1-e^{-\kappa\tau} \quad (2)$$

In this equation, κ is the response coefficient, characteristic of the cell line. After radiation exposure, physical dose generated hits are determined by sampling a Poisson distribution with a mean (Hits/Gy) proportional to the local absorbed dose (D). As explained, additional hits due to the signaling effects are also generated by sampling Poisson distribution with a mean HB (characteristic of the cell line). These hits are caused by direct effects and translate into biological damages. Depending on the level of the accumulated hits, cells may have three potential responses to these damages: 1) if more than 5 hits accumulate in cells, they die immediately. 2) if cells are irradiated in the G1 phase, they may experience arrest by more than 3 hits. 3) in the G2 phase, cells will be killed by even 1 hit. It is necessary to mention that MM576 cells have a deficient p53 that results in a poor G1 checkpoint, and thus the G1 arrest was removed in these cells. Finally, by calculating the percentage of the killed and arrested cells, the percentage of surviving cells is calculated. A detailed description of how damage and its impact on cell survival are calculated can be found in previous studies [22-24].

Three-dimensional signaling

Specifically, for each plan under consideration, the DICOM-RT objects including RT Image, RT Structure Set, and RT Dose files were extracted from HT-TPS and imported into a custom MATLAB program (R2015b, The Math Works, Inc., Natick, Massachusetts, USA), which divided the volume under consideration into a series of voxels in 3 dimensions and extracted the dose delivered to each voxel.

Signal production, diffusion, and decay were simulated from a time t=0 when radiation is delivered (ρ_0 = 0) and proceeds in a series of time steps (Δt=1 sec). At each time step, from "t" to "t+(Δt)", the signal level is calculated as follows:

1. An additional signal is produced within voxels with signal production rates of ν, until $t=t_{sig}$. After this time the cells cease signaling and the source of the signal is eliminated.
2. Produced signaling molecules diffuse between other voxels, according to the diffusion equation (3) as follow:

$$\frac{d\rho}{dt} = -D\nabla^2\rho \quad (3)$$

Where D is the diffusion coefficient, ρ is the local signal concentration at each point, and ∇^2 is the Laplacian operator. No signal is generated or diffused outside of the volume.

3. A portion of the signal decays by decay coefficient, λ.

If we consider a one-dimensional diffusion process, the diffusion and signal decay is calculated by equation (4):

$$\frac{\partial\rho}{\partial t} = D\frac{\partial^2\rho}{\partial z^2} - \lambda\rho \quad (4)$$

For simplicity, the spatial variation of the signal in equation (5) is considered as a one-dimensional process and only in the z-direction, which can then be generalized to the three dimensions.

By replacing equation 5 in equation 4, the time evolution can be expressed by equations (6 and 7):

$$\left.\frac{\partial\rho}{\partial t}\right|_{t,z_i} = \frac{D}{\Delta z^2}(\rho_{t,z_{i-1}} + \rho_{t,z_i} - \rho_{t,z_{i+1}}) - \lambda\rho_{t,z_i} \quad (6)$$

$$\rho_{t+\Delta t,z_i} = \rho_{t,z_i} + \Delta t\left.\frac{\partial\rho}{\partial t}\right|_{t,z_i} \quad (7)$$

In this equation, Δt is the time step. As mentioned, equation (7) can be numerically implemented and used to simulate the time evolution of the signal where the signal concentration changes in only one direction due to one-dimensional diffusion. By dividing the desired volume into a three-dimensional array of voxels, the signal distribution in three dimensions can be easily calculated by considering the three-dimensional Laplacian by equation (8):

$$\nabla^2\rho = \frac{\partial^2\rho}{\partial x^2} + \frac{\partial^2\rho}{\partial y^2} + \frac{\partial^2\rho}{\partial z^2} \quad (8)$$

In this equation, each partial spatial derivative can be approximated as above. This model proceeds until the signaling is ceased and the maximum concentration in all voxels fell below the response threshold. The total time that the signal level has been above the response threshold is calculated for each voxel and is translated to the signaling-induced damage using a modified version of the sample McMahon's code, written in the Python environment (Python Software Foundation, Beaverton, OR, USA). Then, the total level of damages and thus the survival probabilities are calculated by combining direct damage and indirect signaling effect, as outlined earlier.

A big challenge with the *in-vitro/in-vivo* translation is that the rate of diffusion is currently poorly characterized. We cannot measure the signal kinetics *in-vivo*. So, we made some assumptions about this parameter. Here, the diffusion coefficient (D) was

[DOI: 10.52547/ijrr.20.3.20]

characterized in terms of its equilibrium range (r). The relationship between these parameters can be expressed using equation (9):

$$r = \sqrt{\frac{D}{\lambda}} \quad (9)$$

In this work, the diffusion coefficient was set to model various signaling ranges from 0 to 20 mm. This leads to a rational coefficient for a simple homogeneous diffusion process. Larger diffusion ranges may involve other dispersive processes, that lie beyond the scope of this study.

Dose quantification

To investigate the impact of the bystander signal on dose-volume histograms (DVHs), signaling-adjusted dose (D_{sig}) distribution was calculated for each plan and signaling range. For each voxel, the predicted survival level using the bystander model (SF) was converted into D_{sig} using equation (10) by calculating the dose which gives the same level of survival in the LQ model.

$$D_{sig} = \frac{-\alpha + \sqrt{\alpha^2 - 4\beta \ln(SF)}}{2\beta} \quad (10)$$

Here α and β are cell-specific parameters of the LQ model for the melanoma cell line (MM576). The cell-specific parameters for the bystander model were taken from McMahon's study [23], giving LQ parameters of α= 0.12, β= 0.005 (R^2=0.9992), as seen experimentally[26].

The physical and signaling-adjusted doses then were converted into equivalent uniform doses (EUDs) for ease of comparison between different treatment plans. The EUD is the dose when homogeneously delivered to a tumor volume would result in the same mean survival fraction as the given heterogeneous irradiation, and is given by equation (11):

$$e^{-(\alpha EUD + \beta EUD^2)} = \sum V_i \, e^{-(\alpha D_i + \beta D_i^2)} \quad (11)$$

Here, V_i is the percentage of the volume receiving the dose D_i, and D_i can be considered either as the physical dose or the signaling-adjusted dose.

In this work, we have investigated how DVHs, dose distribution, EUD, mean dose, and other dosimetric parameters change by incorporating radiation-induced signaling effects in calculations.

RESULTS

Impact on dose distributions

Figure 2. illustrates an example of physical dose distribution (a and d), dose difference plot (b and e), and signalling adjusted dose distribution (c and f) in GTV for a signal range of 20 mm in axial (a-c) and coronal slices (d-f) from the LATTICE treatment plan.

As can be seen, incorporating signaling-driven effects into dose distribution causes a significant deviation from physical dose planning. As can be seen from the dose difference plots, there is an increase in cell killing and thus an increase in signaling-adjusted doses in low dose regions due to signaling from neighboring higher dose regions. Additionally, a small reduction in signaling-adjusted doses is observed in high dose regions, as the signaling concentration falls off more rapidly near steep dose gradients than the uniform irradiation typically assumed in the LQ model. However, this change is relatively minor, with decreases of <5% compared with increases of up to 150% in the LATTICE plane. Similar results were observed for the TOMOGRID plan. Intercellular signaling effects lead to significantly broadening the dose distribution, softening steep dose gradients, and increasing the valley/peak ratio. However, the TOMOGRID plan generally sees lower dose distribution changes than the LATTICE radiotherapy plan.

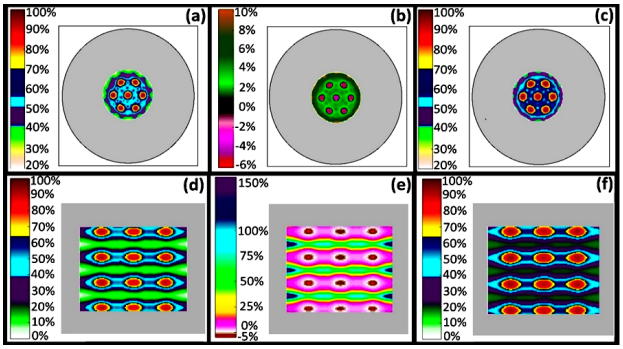

Figure 2. Impact of signalling-driven effects on dose distribution for LATTICE radiotherapy plan, in axial (**a, b,** and **c**) and coronal (**d, e,** and **f**) slices. Figures a and d show physical dose distributions generated from treatment planning system. Figures c and f show the resulting signalling adjusted dose distributions with a signal range of 20 mm. The color bars in these figures show the percent dose. Dose difference maps (**b** and **e**) indicate the percentage of increase or decrease in physical dose due to signalling effects. For example, the purple (in figure **e**) shows the areas that see about a 150% increase in cell killing compared with physical dose alone.

Impact on DVHs

Figure 3. shows the DVH curves for TOMOGRID and LATTICE plans for both physical dose and signaling-adjusted dose with a series of diffusion ranges from 2.5 to 20 mm for GRID target and GRID avoidance volumes.

As would be expected, there is a significant difference between signaling adjusted dose histograms and physical dose histograms for GRID avoidance volumes at the low doses. Cell killing from damaging signals in high dose regions shifts the signaling adjusted DVHs to the right at these doses. This effect is more significant at the LATTICE plan because the dose is spatially fractionated in three dimensions, and thus the steep dose gradients drive

[DOI: 10.52547/ijrr.20.3.20]

the damaging signals more effectively from the high-dose regions to the low-dose regions in all directions. Additionally, as signal ranges increase, the divergence between the model's predictions and physical plan increases, especially in the low dose regions. For the highest dose regions in GRID avoidance volume, only a small increase in signaling adjusted DVHs is observed with increasing signaling range. However, for the GRID target volume increasing ranges lead to a reduction in cell killing in the highest dose regions.

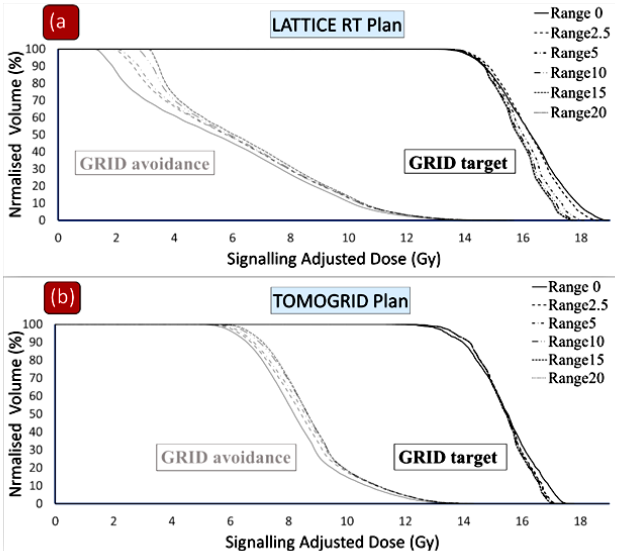

Figure 3. Dose-volume histograms of LATTICE radiotherapy plan **(a)** and TOMOGRID plan **(b)** for GRID target (semi-transparent lines) and GRID avoidance (opaque lines) volumes for either 0-mm range (physical dose) or signalling ranges of 2.5-20 mm.

Impact on mean dose and EUD

Table 1 shows the mean dose, EUD and mean survival fraction (SF) of GTV, GRID avoidance and GRID target volumes for TOMOGRID and LATTICE plans for various signal ranges. In GTV and GRID avoidance volume, an increase in physical mean dose, on the order of 0.8 Gy for the LATTICE plan and 0.5 Gy for the TOMOGRID is seen at 20-mm ranges. By contrast, there is a small reduction in physical mean dose delivered to the GRID target volume, on the order of 0.45 Gy for the LRT and 0.07 Gy for the TOMOGRID at 20-mm ranges. The impact of the intercellular signalling on EUD is similar to that of the mean dose with a little more increase in the physical EUD of the GTV and GRID avoidance.

Table1. Mean dose, mean survival fraction (SF) and EUD of the 3 volumes under consideration for a series of signalling ranges for LRT (**a**) and TOMOGRID (**b**) plans.

Another important dosimetric parameter in SFRT plans that evaluates the heterogeneity of the dose distribution is the valley/peak dose ratio which was defined as the ratio of the mean dose to the GRID avoidance to the mean dose to the GRID target. Figure 5. shows an increase in valley/peak ratio as a function of the signaling range. As discussed, at higher signaling range the damaging signals diffuse away from high dose regions and increase the level of cell killing at low dose regions. This leads to the softening steep dose gradients and an increase in the valley/peak ratio from 0.35 and 0.54 in the physical plan to 0.42 and 0.58 in the signalling range of 20 mm for LRT and TOMOGRID, respectively. As can be seen in figure 5., the LRT plan shows more divergence between physical valley/peak dose ratio and that is predicted from signalling adjusted dose distribution.

(a)	LATTICE RT Plan								
	GTV			GRID target			GRID avoidance		
Range	mean dose	SF	EUD	mean dose	SF	EUD	mean dose	SF	EUD
0	6.06	0.45	5.32	16.25	0.04	16.06	5.67	0.47	5.11
2.5	6.50	0.42	5.80	16.22	0.04	16.08	6.13	0.43	5.60
5	6.55	0.41	5.88	15.99	0.04	15.87	6.19	0.43	5.67
10	6.73	0.39	6.09	15.87	0.04	15.77	6.38	0.41	5.90
15	6.87	0.38	6.25	15.82	0.04	15.72	6.53	0.40	6.05
20	6.88	0.38	6.26	15.80	0.04	15.70	6.54	0.40	6.07
(b)	TOMOGRID Plan								
	GTV			GRID target			GRID avoidance		
Range	mean dose	SF	EUD	mean dose	SF	EUD	mean dose	SF	EUD
0	9.10	0.24	8.64	15.42	0.05	15.27	8.38	0.26	8.19
2.5	9.32	0.23	8.85	15.40	0.05	15.28	8.61	0.25	8.40
5	9.40	0.22	8.95	15.39	0.05	15.27	8.71	0.24	8.51
10	9.49	0.22	9.06	15.36	0.05	15.25	8.81	0.24	8.62
15	9.52	0.22	9.09	15.35	0.05	15.24	8.84	0.24	8.66
20	9.53	0.22	9.10	15.35	0.05	15.24	8.85	0.24	8.67

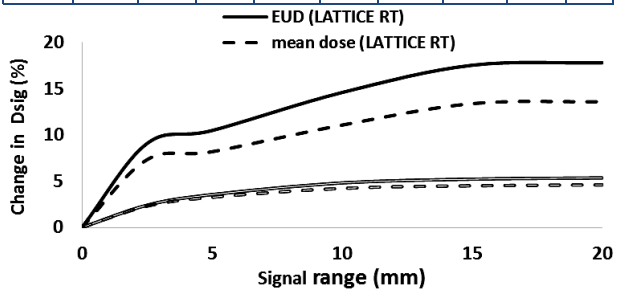

Figure 4. Relative change in signalling adjusted mean dose (dashed lines) and EUD (solid lines) of the GTV compared with the physical plan (0 mm range) for LRT (double lines) and TOMOGRID (dashed double line) plans.

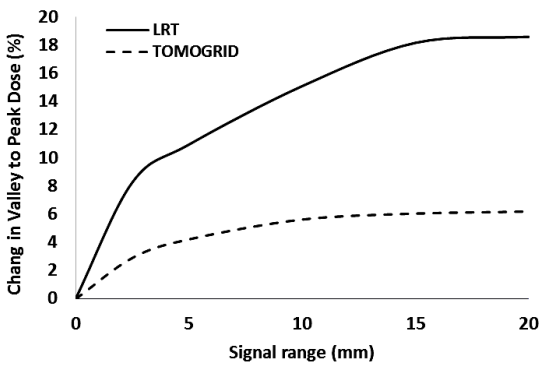

Figure 5. Relative change in valley-to-peak dose ratio for LRT (solid line) and TOMOGRID (dashed line) plan when considering intercellular signalling compared with physical dose alone.

[DOI: 10.52547/ijrr.20.3.20]

DISCUSSION

Radiation therapy treatment plans are optimized typically based on the assumption that the probability of cell killing at a given point depends solely on local absorbed dose, and the cells respond independently to ionizing radiation. Radiation treatments that are planned based on this assumption are effective in treating different cancers when relatively uniform radiation fields are used. However, the role of the intercellular signaling effects in the cellular response cannot be ignored in the complex spatially modulated treatment fields in SFRT. In these highly modulated beams, indirect effects of the intercellular bystander signals become increasingly important and may yield very different results from that are predicted by the traditional radiobiology paradigm [1, 17]. For example, although a highly non-uniform dose distribution and the large dose valleys in the GRID radiation fields are expected to increase the risk of tumor control loss significantly, a uniform tumor mass regression has been observed clinically [27, 28]. Despite there is no doubt that the bystander effects play a key role in non-uniform radiation fields [10, 14, 15, 29], they are not incorporated into the standard LQ model. The experimental results show that the LQ model may not suit the SFRT [14, 15]. In this work, we modeled the tumor response in two ways, (a) through a bystander model that has proved to have good predictive validity in modeling *in-vitro* experiments [22, 23], and (b) through the conventional LQ model that focuses exclusively on the effect of direct irradiation.

This study makes several predictions that may influence decisions about treatment planning. One of the most important is that the cell-killing within the low dose regions in GRID fields depends on signaling from adjacent high dose regions. This view is supported by a recent *in-vitro* study that indicated that the effects such as cell death, DNA damage, formation of the micronucleus and Gamma H2AX foci, and expression of the genes involved in DNA damage repair (Xrcc6 and H2afx) are significantly higher in partially irradiated cells within the shielded area of the GRID field than the cells exposed to the identical uniform does [11]. From figure 2., it can be seen that incorporating signaling effects leads to a significant increase in the cell-killing within low dose regions compared to the physical plan, which leads to a higher EUD and mean dose across the GTV. Several experimental works support these results. In a study, Peng *et al.* measured the survival fraction of the cells in MLC-based GRID radiation fields and observed that the cancer cell survivals in modulated fields were much less than that predicted by the LQ model. However, they found that their extended model, which takes the bystander effect into account, is superior to the standard LQ model in calculating the overall cells survival in the non-uniform radiation fields [14].

Similarly, Butterworth *et al.* found that the LQ model over-predicts the survival fraction of the cells in the shielded area where cells received only the scatter radiation dose [16, 29]. Additionally, the evidence of the bystander response in GRID irradiation and its impact on the EUD and cell survival of the human carcinoma cell line has been demonstrated using both theoretical models and experimental examinations in a recent study by Pakniyat *et al.* [12]. They showed that the EUD predicted by the LQ model for a GRID dose of 10 Gy does not result in the same survival in the open field. The clonogenic survival in GRID beams was less than that measured for the open radiation field with EUD, implying that LQ calculations were unreliable in GRID radiation fields. Moreover, it was shown that the cell-killing from the bystander effect in the GRID field was approximately 2.91 times more than the open field, prominently highlighting the importance of the bystander response in the GRID field.

LRT appears to cause systematically larger cell killing from indirect effects in GTV at all signaling ranges compared with TOMOGRID. In the same way, the cell-killing within the target volume of the LRT plan shows a more dependence on signaling effect than TOMOGRID. Thus, it can be seen that the degree of divergence between the LQ model and bystander model in the calculation of the EUD and mean dose is larger in the LATTICE plan (with more than 20% relative difference in EUD and mean dose). While the divergence is relatively small for the TOMOGRID plan (with an increase <5% in EUD and mean dose). In the TOMOGRID plan, the dose is spatially fractionated only in X-Y planes. However, in LRT, dose gradients exist in all directions and, therefore, bystander signals are being driven away from the high dose regions to the low dose regions more effectively. This results in higher survival in high dose regions and a further reduction in overall survival in the LRT plan. By the present results, previous studies have demonstrated a significant departure of the LQ model from experimental results in fields containing high dose gradients [14, 17]. Similarly, it has been shown that as the mean dose gradient increases, the divergence between LQ model predictions and predictions from the models incorporating bystander effects increases [17].

The predicted EUD and mean dose show a dependence on the signaling range. As shown in figure 4, at short ranges, the EUD and mean dose of GTV increase rapidly as the signaling range increases. However, these effects begin to saturate at high signaling ranges. This can be because the GTV volume is entirely exposed to the damaging signals from high dose regions at the highest signaling range. In the same way, a more rapid signal fall-off is seen in target volume at higher signaling ranges than the no-signaling cases. This leads to a reduction in the signaling adjusted mean dose of the target volume because the rate at which the signal escapes from the

[DOI: 10.52547/ijrr.20.3.20]

voxel, which contains a high physical dose, increases as a function of increasing signal range. Similar results were reported for the DU-145 prostate cancer cell line in a study by Butterworth *et al.* [30]. They generated several spatially fractionated treatment plans using the small-animal radiotherapy research platform and calculated the survival fraction and EUD for different signaling ranges. Similar to our results, it was shown that the increase in the EUD builds up rapidly at low ranges and begins to saturate at higher ranges.

While the current theoretical study modeling potential impacts of the signaling driven effects on the radiobiological response of melanoma to SFRT, clinical validation of these effects is challenging. Much uncertainty still exists about many parameters of the current model [24, 30]. One of the most noticeable of these is a detailed definition of the signaling itself because the assumption of simple linear diffusion is a simplification. Another major source of uncertainty is in the characterization of the *in-vivo* range of these signals due to the lack of adequate support from experimental studies. Further investigations that more precisely quantify these effects need to be undertaken, both in vivo and in vitro, to confirm and validate these findings by testing them against different cancer types and SFRT plans. Validating these findings in vivo will be an important step before it can guide clinical planning and generate clinical predictions.

CONCLUSION

This work indicated that the survival in spatially fractionated radiotherapy plan is strongly affected by the radiation-induced signals, and the conventional LQ model cannot predict these effects well. Therefore, it is recommended to use the radiobiological models which take both the signaling and radiation effects into account to predict survival in highly modulated radiation beams, especially in LATTICE radiotherapy, which contains high dose gradients in three dimensions.

ACKNOWLEDGEMENTS

The authors would like to thank Dr McMahon for his helpful guidance on various technical issues examined in this paper.

***Funding*:** This work is a part of a PhD thesis (No: 399019) which was financially supported by the Isfahan University of Medical Sciences, Isfahan, Iran.

***Ethical compliance*:** This article does not contain any studies with human participants or animals performed by any of the authors. The Research Ethics Committee of Isfahan University of Medical Sciences-School of Medicine has confirmed the ethical code of IR.MUI.MED.REC.1399.119.

***Conflicts of Interests*:** The authors declare that they have no conflicts of interest.

***Authors contribution*:** Study conception and design: F. Mahmoudi, D. Shahbazi-Gahrouei, N. Chegeni. Data collection and software: F. Mahmoudi, M. Saeb, V. Sadeghi, S. Hemati. Analysis and interpretation of results: F. Mahmoudi, D. Shahbazi-Gahrouei, N. Chegeni and finally draft manuscript preparation: F. Mahmoudi, D. Shahbazi-Gahrouei, N. Chegeni.

REFERENCES

1. Mahmoudi F, Shahbazi-Gahrouei D, Chegeni N (2021) The role of the spatially fractionated radiation therapy in the management of advanced bulky tumors. *PJMPE,* ***27****(2): 123-35.*
2. Gholami S, Nedaie HA, Longo F, Ay MR, Wright S, Meigooni AS (2016) Is grid therapy useful for all tumors and every grid block design? *J Appl Clin Med Phys,* ***17****(2).*
3. Gholami S, Nedaie HA, Longo F, Ay MR, Dini SA, Meigooni AS (2017) Grid block design based on monte carlo simulated dosimetry, the linear quadratic and Hug–Kellerer radiobiological models. *Journal of Medical Physics,* ***42****(4): 213.*
4. Zhang H, Zhong H, Barth RF, Cao M, Das IJ (2014) Impact of dose size in single fraction spatially fractionated (grid) radiotherapy for melanoma. *Medical physics,* ***41****(2): 021727.*
5. Meigooni AS, Dou K, Meigooni NJ, Gnaster M, Awan S, Dini S, *et al.* (2006) Dosimetric characteristics of a newly designed grid block for megavoltage photon radiation and its therapeutic advantage using a linear quadratic model. *Medical physics,* ***33****(9): 3165-73.*
6. Sheikh K, McNutt T, Bell L, Moore J, Hrinivich W, Teslow T, *et al.* (2018) Comparison of Treatment Planning Approaches for Spatially Fractionated Irradiation of Deep Tumors. *Int J Radiat Oncol Biol Phys,* ***102****(3): e499.*
7. Sathishkumar S, Dey S, Meigooni AS, Regine WF, Kudrimoti M, Ahmed MM, *et al.* (2002) The impact of TNF-α induction on therapeutic efficacy following high dose spatially fractionated (GRID) radiation. *Technol Cancer Res Treat,* ***1****(2): 141-7.*
8. Kanagavelu S, Gupta S, Wu X, Philip S, Wattenberg MM, Hodge JW, *et al.* (2014) *In vivo* effects of lattice radiation therapy on local and distant lung cancer: potential role of immunomodulation. *Radiat Res,* ***182****(2): 149-62.*
9. Asur RS, Sharma S, Chang C-W, Penagaricano J, Kommuru IM, Moros EG, *et al.* (2012) Spatially fractionated radiation induces cytotoxicity and changes in gene expression in bystander and radiation adjacent murine carcinoma cells. *Radiat Res,* ***177****(6): 751 -65.*
10. Asur R, Butterworth KT, Penagaricano JA, Prise KM, Griffin RJ (2015) High dose bystander effects in spatially fractionated radiation therapy. *Cancer Lett,* ***356****(1): 52-7.*
11. Pakniyat F, Nedaie HA, Mozdarani H, Mahmoudzadeh A, Salimi M, Griffin RJ, *et al.* (2020) Enhanced response of radioresistant carcinoma cell line to heterogeneous dose distribution of grid; the role of high-dose bystander effect. *Int J Radiat Biol,* ***96****(12): 1585-96.*
12. Pakniyat F, Gholami S, Nedaie H, Mozdarani H, Mahmoudzadeh A, Salimi M (2020) Demonstration of bystander response in high dose technique of grid using theoretical calculation by linear quadratic model along with experimental investigations. *Int J Radiat Res,* ***18*** *(3): 495-504.*
13. Zwicker RD, Meigooni A, Mohiuddin M (2004) Therapeutic advantage of grid irradiation for large single fractions. *IJROBP,* ***58****(4): 1309-15.*
14. Peng V, Suchowerska N, Rogers L, Claridge Mackonis E, Oakes S, McKenzie DR (2017) Grid therapy using high definition multileaf collimators: realizing benefits of the bystander effect. *Acta Oncol,* ***56****(8): 1048-59.*
15. Peng V, Suchowerska N, Esteves ADS, Rogers L, Mackonis EC, Toohey J, *et al.* (2018) Models for the bystander effect in gradient radiation fields: Range and signalling type. *Journal of Theoretical Biology,* ***455:*** *16-25.*
16. Butterworth KT, McGarry CK, Trainor C, McMahon SJ, O'Sullivan JM, Schettino G, *et al.* (2012) Dose, dose-rate and field size effects on cell survival following exposure to non-uniform radiation fields. *Phys Med Biol,* ***57****(10): 3197.*
17. Mahmoudi F, Chegeni N, Bagheri A, Asl JF, Batiar MT (2021) Impact of radiobiological models on the calculation of the therapeutic

[DOI: 10.52547/ijrr.20.3.20]

parameters of Grid therapy for breast cancer. *Applied Radiation and Isotopes,* ***174:*** *109776.*
18. Yan Y, Dou Y, Weng X, Wallin A (2010) SU-GG-T-256: An Enhanced DICOM-RT Viewer. *Medical Physics,* ***37****(6Part19): 3244.*
19. Sheikh K, Hrinivich WT, Bell LA, Moore JA, Laub W, Viswanathan AN, *et al.* (2019) Comparison of treatment planning approaches for spatially fractionated irradiation of deep tumors. *J Appl Clin Med Phys,* ***20****(6): 125-33.*
20. Zhang X, Penagaricano J, Yan Y, Liang X, Morrill S, Griffin RJ, *et al.* (2016) Spatially fractionated radiotherapy (GRID) using helical tomotherapy. *J Appl Clin Med Phys,* ***17****(1).*
21. Zhang X, Penagaricano J, Yan Y, Sharma S, Griffin R, Hardee M, *et al.* (2014) Application of spatially fractionated radiation (GRID) to helical tomotherapy using a novel TOMOGRID template. *Technol Cancer Res Treat: tcrtexpress. 2013.600261.*
22. McMahon SJ, Butterworth KT, McGarry CK, Trainor C, O'Sullivan JM, Hounsell AR, *et al.* (2012) A computational model of cellular response to modulated radiation fields. *IJROBP,* ***84****(1): 250-6.*
23. McMahon SJ, Butterworth KT, Trainor C, McGarry CK, O'Sullivan JM, Schettino G, *et al.* (2013) A kinetic-based model of radiation-induced intercellular signalling. *PLoS One,* ***8****(1): e54526.*
24. McMahon SJ, McGarry CK, Butterworth KT, Jain S, O'Sullivan JM, Hounsell AR, *et al.* (2015) Cellular signalling effects in high precision radiotherapy. *Physics in Medicine and Biology,* ***60****(11): 4551.*
25. Partridge M (2008) A radiation damage repair model for normal tissues. *Phys Med Biol,* ***53****(13): 3595.*
26. Ebert MA, Suchowerska N, Jackson MA, McKenzie DR (2010) A mathematical framework for separating the direct and bystander components of cellular radiation response. *Acta Oncol,* ***49****(8): 1334-43.*
27. Huhn JL, Regine WF, Valentino JP, Meigooni AS, Kudrimoti M, Mohiuddin M (2006) Spatially fractionated GRID radiation treatment of advanced neck disease associated with head and neck cancer. *Technol Cancer Res Treat,* ***5****(6): 607-12.*
28. Peñagarícano JA, Moros EG, Ratanatharathorn V, Yan Y, Corry P (2010) Evaluation of spatially fractionated radiotherapy (GRID) and definitive chemoradiotherapy with curative intent for locally advanced squamous cell carcinoma of the head and neck: initial response rates and toxicity. *IJROBP,* ***76****(5): 1369-75.*
29. Butterworth KT, McGarry CK, Trainor C, O'Sullivan JM, Hounsell AR, Prise KM (2011) Out-of-field cell survival following exposure to intensity-modulated radiation fields. *IJROBP,* ***79****(5): 1516-22.*
30. Butterworth KT, Ghita M, McMahon SJ, Mcgarry CK, Griffin RJ, Hounsell AR, *et al.* (2017) Modelling responses to spatially fractionated radiation fields using preclinical image-guided radiotherapy. *Brit J Radiol,* ***90****(1069): 20160485.*

[DOI: 10.52547/ijrr.20.3.20]